

Article

Spin-Phonon Coupling in A_2BMnO_6 ($A = \text{La, Pr, Nd, Sm, Gd}$; $B = \text{Co, Ni}$) Double-Perovskite Thin Films: Impact of the A-Site Cation Radius

Christoph Meyer ¹, Philipp Ksoll ¹, Vladimir Roddatis ^{2,3} and Vasily Moshnyaga ^{1,*}

¹ Erstes Physikalisches Institut, Georg-August-Universität Göttingen, Friedrich-Hund-Platz 1, 37077 Göttingen, Germany; christoph.meyer@phys.uni-goettingen.de (C.M.); philipp.ksoll@stud.uni-goettingen.de (P.K.)

² Institut für Materialphysik, Georg-August-Universität Göttingen, Friedrich-Hund-Platz 1, 37077 Göttingen, Germany; vladimir.roddatis@gfz-potsdam.de

³ GFZ German Research Centre for Geosciences, Helmholtz Centre Potsdam, Telegrafenberg, 14473 Potsdam, Germany

* Correspondence: vmosnea@gwdg.de

X-ray diffraction (XRD) measurements of the $A_2\text{CoMnO}_6$ and $A_2\text{NiMnO}_6$ thin films

In Figure S1 the XRD patterns (θ - 2θ mode, Cu- $K\alpha$ radiation, Bruker AXS D8 Advance) of the $A_2\text{CoMnO}_6$ (a) and $A_2\text{NiMnO}_6$ (b) ($A = \text{La, Pr, Nd, Sm, Gd}$) double perovskite thin films (thickness $d \sim 100$ nm), grown on $\text{SrTiO}_3(111)$ (STO) substrates are shown around the STO(111) reflex for better clarity. XRD patterns for all studied double perovskite films show only reflexes with (111) orientation, confirming the out-of-plane film epitaxy in (111) direction for all the double perovskite films.

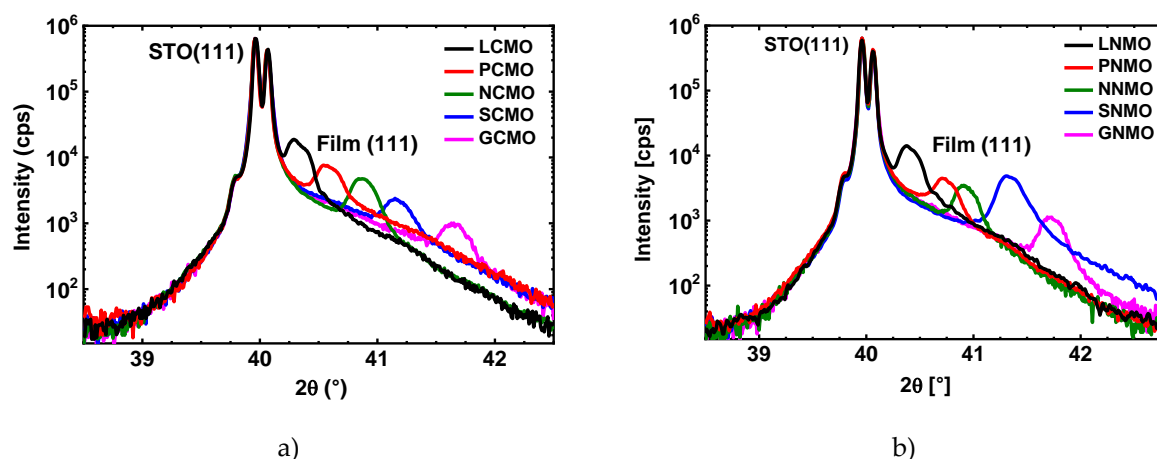


Figure S1. XRD patterns of **a)** $A_2\text{CoMnO}_6/\text{STO}(111)$ and **b)** $A_2\text{NiMnO}_6/\text{STO}(111)$ ($A = \text{La, Pr, Nd, Sm, Gd}$) double perovskite thin film series (thickness $d \sim 100$ nm) around the STO (111) reflex.

Transmission Electron Microscopy (TEM) characterization

In Figure S2 we present a high angle annular dark field (HAADF) image of a representative $\text{Nd}_2\text{CoMnO}_6(111)/\text{STO}(111)$ (NCMO) film. A low magnification HAADF image with selected area electron diffraction confirm epitaxial growth of the 100 nm thick NCMO film and the flat film/substrate interface. A high resolution HAADF image reveals a coherent epitaxial character of the NCMO/STO interface. The weak superstructure spots in the FFT patterns from the NCMO film (top) and STO substrate (bottom) show the presence of Mn/Co cation ordering.

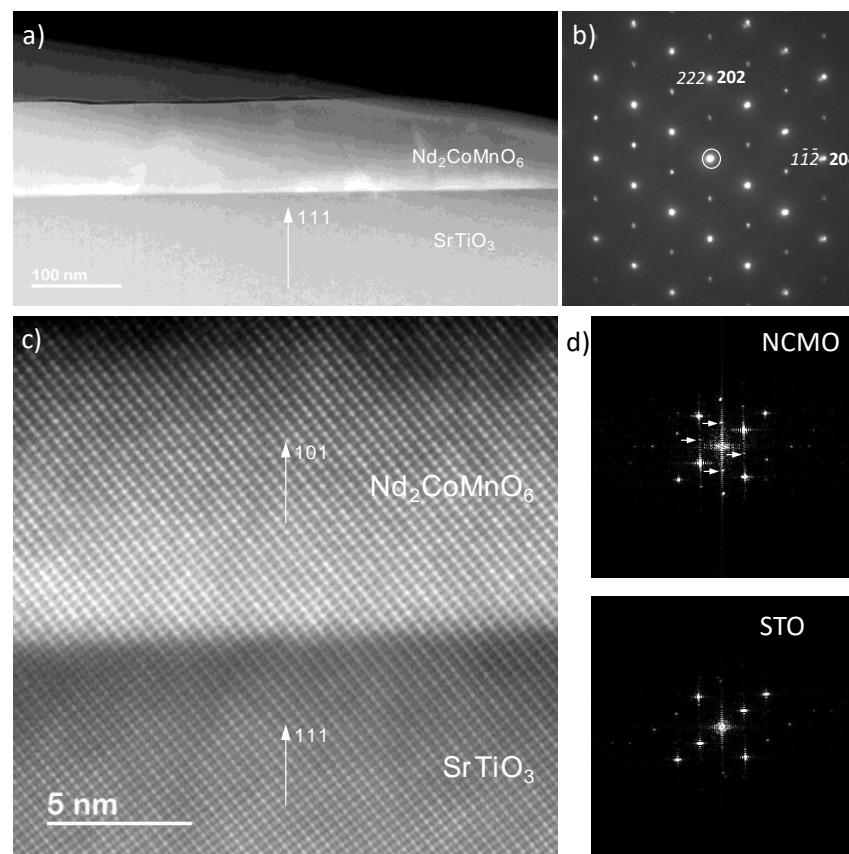


Figure S2. **a)** A low magnification High Angle Annular Dark Field (HAADF) image of $\text{Nd}_2\text{CoMnO}_6$ thin film; **b)** A Selected Area Electron Diffraction (SAED) pattern confirms epitaxial growth of the film; **c)** A high resolution HAADF image of NCMO/STO interface; **d)** FFT patterns from the NCMO film (top) and STO substrate (bottom). The weak superstructure spots marked with the white arrows in the FFT from the NCMO film show the presence of Mn/Co cation ordering.

Magnetization measurements of the A_2CoMnO_6 and A_2NiMnO_6 thin films

Figure S3 displays the temperature dependence of magnetization, $M(T)$, measured at external field $H=1$ kOe of the $\text{A}_2\text{CoMnO}_6/\text{STO}$ (111) ($A = \text{La, Pr, Nd, Sm, Gd}$) double perovskite film series. One can see that all films exhibit paramagnetic-to-ferromagnetic transition with the corresponding Curie temperatures, T_c , calculated from the minimum of the temperature coefficient of magnetization, $\text{TCM} = (1/M)(dM/dT)$. The obtained T_c values are in agreement with previous results for double perovskite A_2CoMnO_6 thin films and bulk samples [1–7] with a high degree of B-site ordering due to ferromagnetic $\text{Co}^{2+}\text{-O-Mn}^{4+}$ super-exchange interaction. Note, that partially B-site disordered A_2CoMnO_6 double perovskites display an additional transition at lower temperatures due to antisite disorder and vibronic $\text{Co}^{3+}\text{-O-Mn}^{3+}$ superexchange interaction [3–7]. Since point defects and antiphase boundaries (APBs) create antiferromagnetic $\text{Co}^{2+}\text{-O-Co}^{2+}$ and $\text{Mn}^{4+}\text{-O-Mn}^{4+}$ interactions, the ferromagnetism for B-site disordered A_2CoMnO_6 double perovskites is weakened. Moreover, one can see a strong difference between the field-cooled (FC) and the zero-field-cooled (ZFC) $M(T)$ curves, indicating, probably, a competition between ferromagnetic and antiferromagnetic interaction for all the A_2CoMnO_6 films [2,4,6,8,9]. This well-known behavior for B-site ordered A_2CoMnO_6 double perovskites [2–5] is assigned to antiphase boundaries (APBs) within the lattice, subdividing antiferromagnetically coupled B-site ordered clusters [2,9]. For the GCMO film an antiferromagnetic coupling of the Gd^{3+} ions with the B-site cations sets in for $T < 50$ K [10].

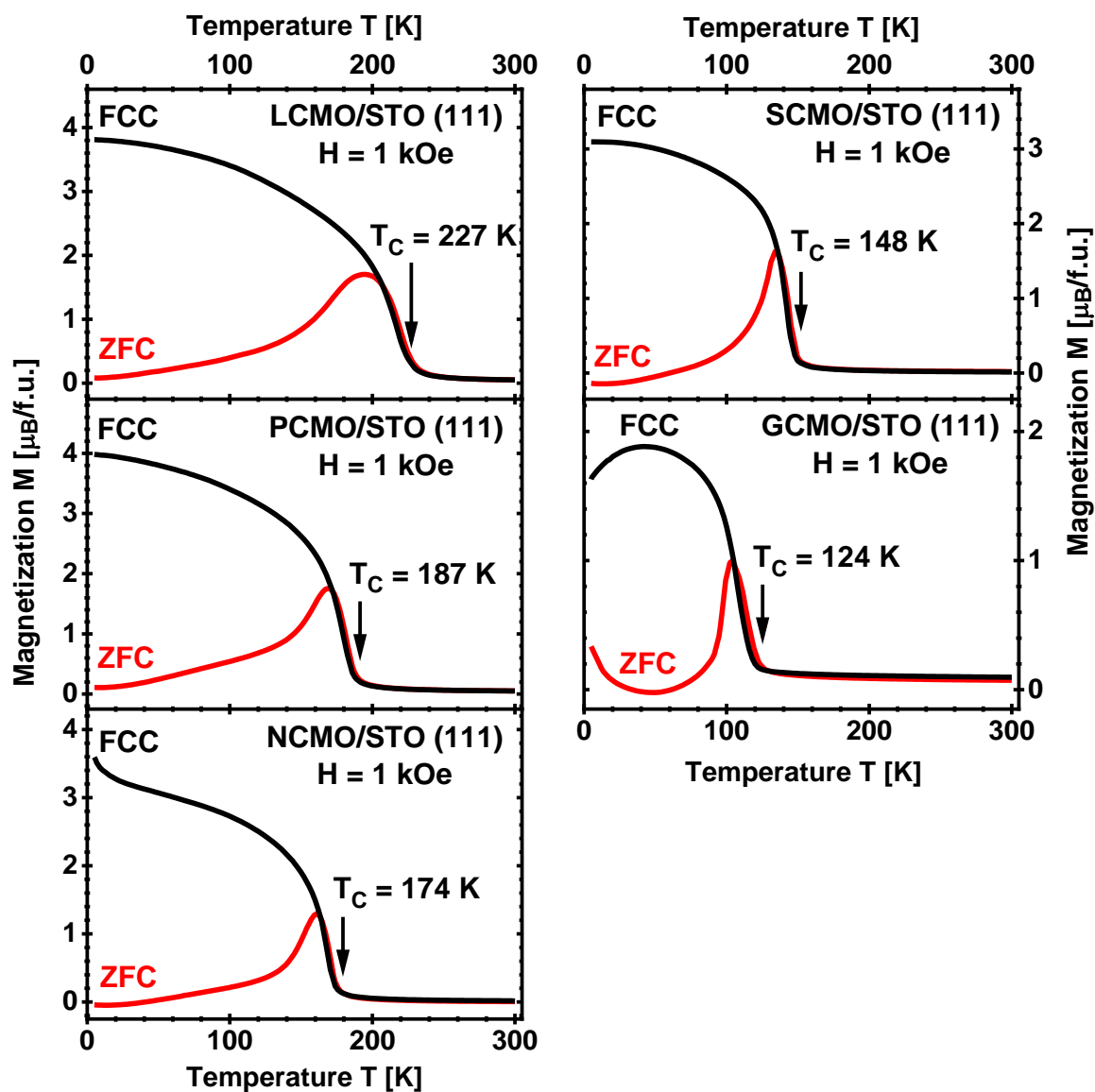


Figure S3. Temperature dependent $M(T)$ magnetization curves (FCC and ZFC, $H=1000$ Oe) of the A_2CoMnO_6/STO (111) ($A = La, Pr, Nd, Sm, Gd$) double perovskite thin film series.

Figure S4 presents the temperature dependent $M(T)$ magnetization curves of the A_2NiMnO_6/STO (111) ($A = La, Pr, Nd, Sm, Gd$) double perovskite film series measured for $H=10$ kOe as field-cooled (FCC) and zero-field-cooled (ZFC) curves. All films exhibit one paramagnetic-to-ferromagnetic transition with Curie temperatures T_c corresponding to previous results for the A_2NiMnO_6 double perovskites [1,11]. The difference between the FCC and ZFC curves is reduced at $H = 10$ kOe. In contrast to the A_2CoMnO_6 series, the discrepancy for the FCC and ZFC curves is already small for $H = 1$ kOe for the A_2NiMnO_6 series, as for example for LNMO [12]. An exception is the NNMO film: here for $T < 30$ K the magnetization decreases due to an antiferromagnetic spin-orbit interaction of the Nd^{3+} cations with the B-site cations [11]. A specific behavior is observed for the GNMO film for temperatures $T < 50$ K with a strong paramagnetic contribution of the Gd^{3+} cations, superimposing the ferromagnetic signal [11,13].

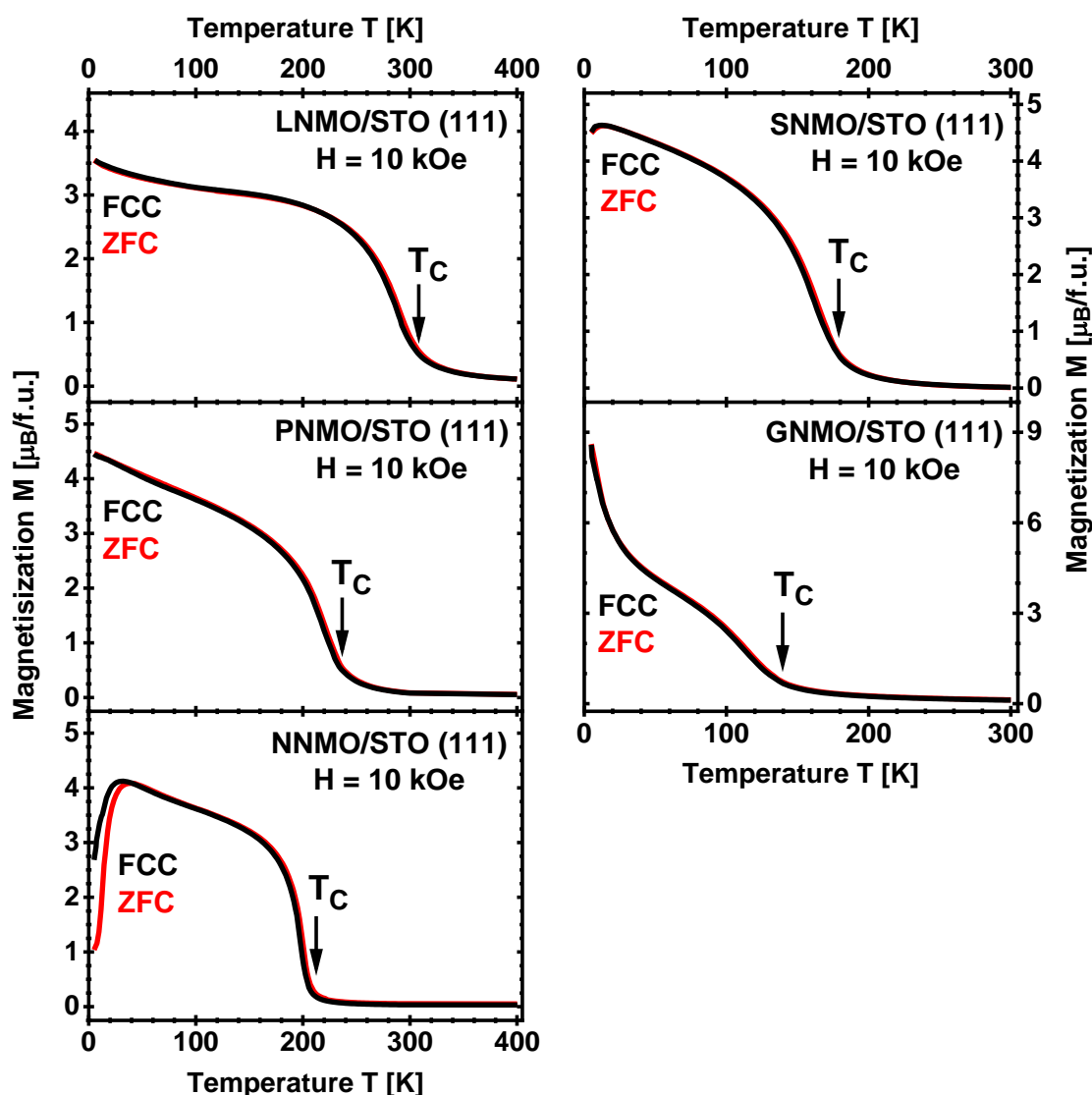


Figure S4. Temperature dependent $M(T)$ magnetization curves (FCC and ZFC, $H=10000$ Oe) of the $A_2\text{NiMnO}_6/\text{STO}$ (111) ($A = \text{La, Pr, Nd, Sm, Gd}$) double perovskite thin film series.

Table S1. Magnetic characteristics of Co- and Ni-series films.

Double perovskite	M_s ($\mu_B/\text{f.u.}$)	M_{Rem} ($\mu_B/\text{f.u.}$)	H_c (kOe)	Double perovskite	M_s ($\mu_B/\text{f.u.}$)	M_{Rem} ($\mu_B/\text{f.u.}$)	H_c (kOe)
LCMO	5.92(10)	3.94(5)	6.8(2)	LNMO	5.00(10)	0.19(5)	0.25(2)
PCMO	6.01(10)	4.73(5)	9.8(2)	PNMO	5.13(10)	0.87(5)	0.55(2)
NCMO	5.81(10)	4.28(5)	10.9(2)	NNMO	5.07(10)	1.28(5)	1.76(2)
SCMO	5.94(10)	4.03(5)	18.1(2)	SNMO	5.07(10)	2.23(5)	1.05(2)
GCMO	18.19(10)	1.56(5)	2.5(2)	GNMO	18.94(10)	1.34(5)	0.45(2)
YCMO	4.75(10)	2.9(5)	22.6(2)	YNMO	5.12(10)	1.19(5)	0.79(2)

References

1. Bull, C.L.; McMillan, P.F. Raman scattering study and electrical properties characterization of elpasolite perovskites $\text{Ln}_2(\text{BB}')\text{O}_6$ ($\text{Ln} = \text{La, Sm, Gd}$ and $\text{B, B}' = \text{Ni, Co, Mn}$). *J. Solid State Chem.* **2004**, *177*, 2323–2328.
2. Kim, M.K.; Moon, J.Y.; Choi, H.Y.; Oh, S.H.; Lee, N.; Choi, Y.J. Investigation of the magnetic properties in double per-ovskite R_2CoMnO_6 single crystals ($\text{R} = \text{rare earth: La to Lu}$). *J. Phys. Condens. Matter* **2015**, *27*, 426002.
3. Dass, R. I.; Goodenough, J.B. Multiple magnetic phases of $\text{La}_2\text{CoMnO}_{6-\delta}$ ($0 < \delta < \sim 0.05$). *Phys. Rev. B* **2003**, *67*, 014401.
4. Egoavil, R.; Hühn, S.; Jungbauer, M.; Gauquelin, N.; Béché, A.; Van Tendeloo, G.; Verbeeck, J.; Moshnyaga, V. Phase problem in the B-site ordering of $\text{La}_2\text{CoMnO}_6$: impact on structure and magnetism. *Nanoscale* **2015**, *7*, 9835–9843, doi:10.1039/c5nr01642h.

5. Meyer, C.; Roddatis, V.; Ksoll, P.; Damaschke, B.; Moshnyaga, V. Structure, magnetism, and spin-phonon coupling in heteroepitaxial $\text{La}_2\text{CoMnO}_6/\text{Al}_2\text{O}_3(0001)$ films. *Phys. Rev. B* **2018**, *98*, 134433, doi:10.1103/physrevb.98.134433.
6. Guo, H.Z.; Gupta, A.; Zhang, J.; Varela, M.; Pennycook, S.J. Effect of oxygen concentration on the magnetic properties of $\text{La}_2\text{CoMnO}_6$ thin films. *Appl. Phys. Lett.* **2007**, *91*, 202509, doi:10.1063/1.2814919.
7. E Kleibeuker, J.; Choi, E.-M.; Jones, E.D.; Yu, T.-M.; Sala, B.; A MacLaren, B.; Kepaptsoglou, D.; Hernandez-Maldonado, D.; Ramasse, Q.M.; Jones, L.; et al. Route to achieving perfect B-site ordering in double perovskite thin films. *NPG Asia Mater.* **2017**, *9*, e406, doi:10.1038/am.2017.113.
8. Bai, Y.; Xia, Y.; Li, H.; Han, L.; Wang, Z.; Wu, X.; Lv, S.; Liu, X.; Meng, J. A-Site-Doping Enhanced B-Site Ordering and Correlated Magnetic Property in $\text{La}_{2-x}\text{Bi}_x\text{CoMnO}_6$. *J. Phys. Chem. C* **2012**, *116*, 16841–16847, doi:10.1021/jp302735x.
9. Wang, X.L.; James, M.R.; Horvat, J.C.; Dou, S.X. Spin glass behaviour in ferromagnetic $\text{La}_2\text{CoMnO}_6$ perovskite manganite. *Supercond. Sci. Technol.* **2002**, *15*, 427–430, doi:10.1088/0953-2048/15/3/328.
10. Murthy, J.K.; Chandrasekhar, K.D.; Mahana, S.; Topwal, D.; Venimadhav, A. Giant magnetocaloric effect in $\text{Gd}_2\text{NiMnO}_6$ and $\text{Gd}_2\text{CoMnO}_6$ ferromagnetic insulators. *J. Phys. D: Appl. Phys.* **2015**, *48*, 355001, doi:10.1088/0022-3727/48/35/355001.
11. Booth, R.; Fillman, R.; Whitaker, H.; Nag, A.; Tiwari, R.; Ramanujachary, K.; Gopalakrishnan, J.; Lofland, S. An investigation of structural, magnetic and dielectric properties of R_2NiMnO_6 (R = rare earth, Y). *Mater. Res. Bull.* **2009**, *44*, 1559–1564, doi:10.1016/j.materresbull.2009.02.003.
12. Dass, R. I.; Yan, J.-Q.; Goodenough, J.B. Oxygen stoichiometry, ferromagnetism, and transport properties of $\text{La}_{2-x}\text{NiMnO}_{6+\delta}$. *Phys. Rev. B* **2003**, *68*, 064415.
13. Oh, S.H.; Choi, H.Y.; Moon, J.Y.; Kim, M.K.; Jo, J.; Lee, N.; Choi, Y.J. Nonlinear magnetodielectric effect in double-perovskite $\text{Gd}_2\text{NiMnO}_6$. *J. Phys. D: Appl. Phys.* **2015**, *48*, 445001.